RSC Advances

PAPER

View Article Online
View Journal | View Issue

Cite this: *RSC Adv.*, 2021, **11**, 24345

Development of biodegradable zein-based bilayer coatings for drug-eluting stents†

Martina Lenzuni,[ab] Giulia Suarato,[ac] Dalila Miele,[d] Riccardo Carzino,[a] Marco Ruggeri,[d] Rosalia Bertorelli,[c] Giuseppina Sandri[d] and Athanassia Athanassiou*[a]

Drug-eluting stents (DES) have been widely used for the treatment of cardiovascular diseases. Nevertheless, chronic inflammation and delayed re-endothelialization still represent challenges for their clinical use. In the present work, we developed novel bilayer coatings for stent applications that could overcome these limitations, exclusively using biodegradable plant-based drugs and polymers. In particular, stainless steel surfaces were coated with rutin-loaded zein (the active layer) and cross-linked alginate (the sacrificial layer) *via* facile dip and spray coating methods. Various mechanical tests and analysis tools, such as infrared spectroscopy, water contact angle measurements, and scanning electron microscopy were used to characterize the coated surfaces. Degradation and release studies of the films were extensively carried out and compared. The release rate of rutin from the bilayer coating reached 66.1 ± 3.2% within 24 hours of incubation (initial burst period), while the rest of the drug was released over 21 days in a sustained manner. Antioxidant assays confirmed that rutin retained its free radical scavenging ability after being eluted in phosphate buffer at 37 °C. *In vitro* results with human fibroblasts and endothelial cells suggested that the coating materials and their degradation products are highly biocompatible. In conclusion, our novel drug-eluting coatings, fabricated with natural biodegradable polymers, are promising materials for DES applications, allowing a sustained drug delivery and improving the biocompatibility of cardiovascular implanted devices.

Received 13th May 2021
Accepted 29th June 2021

DOI: 10.1039/d1ra03748j

rsc.li/rsc-advances

1 Introduction

Cardiovascular diseases continue to be the leading cause of mortality worldwide, accounting for 46% of all deaths in Europe alone, with a vast majority of these deaths attributed to obstructive coronary artery disease (CAD).[1] The main cause of CAD is the deposition of fat and cholesterol within the artery walls, which eventually leads to the narrowing, or "stenosis", of the arteries. This subsequently causes a reduction of the blood flow, thus impeding the supply of oxygen and nutrients to the surrounding tissues. A coronary stent is a cylindrical metal mesh that is introduced into the lumen of the blocked artery and it is expanded at the level of the obstruction until its diameter is equal to that of the original vessel, allowing restoration of a regular blood flow. Unfortunately, stent application often results in substantial blood vessel wall damage and endothelium destruction, which may induce a cascade of inflammatory events that leads to in-stent restenosis (ISR) of the tissues in contact with the metal device. The rate of ISR reaches 30% in patients receiving this type of coronary surgery, mainly due to unsuitable biocompatibility of the bare metal stents (BMS).[2] The shortcomings of BMS, in particular the high rate of ISR, have led to the development of new stent surface treatments and coatings, and, in 1999, the first model of drug-eluting stent (DES) was implanted. The carrier, usually a polymer matrix, retains the chosen drug, maintains its chemical stability, and, most importantly, controls its release kinetics. The aim is to timely deliver the therapeutic agent to the target position, at a precise concentration over a relatively long period of time.[3] Certainly, one of the fundamental features of a stent, a device that must remain in the body for a prolonged time, is biocompatibility. Several DES are fabricated with synthetic polymers ("first-generation DES") that serve as drug delivery carriers for the elution of the active agent over time. Despite several clinical trials have endorsed the effectiveness of DES over BMS in blocking restenosis (risk of ISR reduced down to 10%), long-term follow-up studies have documented an increased risk of late stent thrombosis due to delayed vascular healing and re-endothelialization in patients following first-generation DES implantation.[4,5] The permanent presence of the synthetic polymer coating often leads to complications such

[a]*Smart Materials Group, Istituto Italiano di Tecnologia, via Morego 30, 16163 Genoa, Italy. E-mail: martina.lenzuni@iit.it*

[b]*DIBRIS, University of Genoa, via Opera Pia 13, Genoa, Italy*

[c]*Translational Pharmacology, Istituto Italiano di Tecnologia, via Morego 30, 16163 Genoa, Italy*

[d]*Department of Drug Sciences, University of Pavia, viale Taramelli 12, 27100 Pavia, Italy*

† Electronic supplementary information (ESI) available. See DOI: 10.1039/d1ra03748j

as chronic inflammation and adverse response at the implant site.[6] Moreover, non-permanent, synthetic polymers, *i.e.* poly-(lactic-*co*-glycolic acid) (PLGA) and poly-L-lactide acid (PLLA), generate degradation products that can cause a local inflammatory response and delay tissue healing due to acidic by-products.[7,8]

Recently, the use of naturally derived materials, which integrate non-toxicity with other significant properties, such as biodegradability and biocompatibility, has attracted scientific interest. In fact, biopolymers of natural origin typically degrade physiologically to substances of low molecular weight, which can be easily excreted by the body, subsequently developing less inflammation in long-term applications.[8,9] Bio-based polymers such as collagen, silk, hyaluronic acid, and chitosan have been reported as coating materials for stents and some of them have demonstrated good properties, such as controlled drug release, low cytotoxicity, and hemocompatibility.[10–13] However, many of these materials present some disadvantages (thrombogenicity, low mechanical resistance, mild immunogenicity, and high cost in order to obtain pure polymers).[14,15]

Sodium alginate, a natural polysaccharide found in seaweed, has been studied for biomedical applications (*i.e.* drug delivery or wound healing) due to its hydrophilicity, high biocompatibility, and low immune response. In addition, sodium alginate can be rapidly cross-linked to form gel networks in the presence of calcium ions, thus enabling the encapsulation of active biomolecules. Providing a hydrophilic interface between a device surface and the tissue fluids, alginate can form coatings that could minimize tissue reactions caused by the device implantation and prevent non-specific adsorption of blood proteins and platelets.[16]

Plant-based proteins have recently appeared as new biomaterials with the ability to deliver drugs, proteins, and DNA fragments.[17] In comparison to animal proteins, which may face health risks, plant proteins are considered to have plenty of benefits, ranging from biodegradability, biocompatibility, abundant supply, and readily availability, to low fabrication costs and environmental impact. Zein is a promising plant-derived protein extracted from renewable resources. This biodegradable and biocompatible major storage protein of corn has been increasingly considered for biomedical applications.[18] In 1985, zein was licensed by the USA Food and Drug Administration (www.fda.gov) as a generally recognized as safe (GRAS) excipient for film coating of pharmaceuticals, primarily comprising tablets, based on the long history of zein use in food.[19] The potential of zein as a matrix material in the pharmaceutical industry for controlled release applications has been recently investigated, due to its solubility in aqueous alcohol solutions but not in water.[20–22] Zein has been shown to be cell- and hemocompatible and to lead to degradation products that can enhance cell proliferation.[23,24] In addition, part of the N-terminal peptide region of zein has been shown to interact with cell membranes and to act as a peptides vehicle across those barriers.[25] Zein can be quickly transformed into a range of shapes and structures, including films, nanoparticles, and fibers.[20,26] Several molecules and drugs have been incorporated and tested for their release from zein matrices, such as essential oils, dyes, and anti-microbial agents.[18,27,28]

Different classes of drugs have been evaluated and employed for DES applications, such as anti-restenotic (*e.g.* sirolimus and paclitaxel), anti-inflammatory (*e.g.* dexamethasone and probucol), and anti-thrombotic (*e.g.* heparin) drugs. Despite the broad spectrum of compounds, many of the currently licensed drugs are considered toxic compounds and pose substantial risks of adverse consequences.

In the plant kingdom, with 9000 structural forms, flavonoids are known to be the largest group of polyphenolic compounds. The considerable interest in flavonoids arises from their numerous biological activities, as they have gained recognition as potential risk-reducing elements for cardiovascular as well as neurodegenerative diseases.[29,30] Rutin, also known as quercetin-3-rutinoside, offers significant pharmaceutical efficacy as an antioxidant, anti-inflammatory, and antiplatelet compound.[31,32] Moreover, rutin and its derivatives can also improve vascular functions and accelerate re-endothelialization.[33] Rutin may be therefore an ideal candidate for future DES coatings, which could potentially prevent the risk of late thrombosis and inflammatory events, reduce oxidative stress in the surrounding tissues, and promote endothelial repair.

In the present work, a double-layer coated 316L stainless steel substrate for stent applications was fabricated and characterized. The coating consists of an active layer (a rutin-loaded zein matrix) and a sacrificial layer (cross-linked alginate), the latter providing a more controlled and sustained release of the active compound. The exclusive use of green solvents and natural polymers of which the coating is composed can ensure biocompatibility, promotion of cell proliferation, and sustained release. Rutin release and antioxidant profiles, together with the physico-chemical properties of both single and double-layer coatings were studied under physiological conditions. The biocompatibility of the fabricated system was examined by evaluating the adhesion and proliferation of endothelial cells and fibroblasts onto each polymeric substrate. Our designed double-layer coating, based on the innovative use of plant-based, biodegradable polymers, constitutes a promising alternative to permanent DES coating, as it shows ideal biocompatibility properties needed to promote appropriate vascular healing.

2 Materials and methods

2.1 Materials

Pure zein powder, rutin hydrate, alginic acid sodium salt, poly(ethylene glycol), 2,2-diphenyl-1-picrylhydrazyl free radical (DPPH$^{\bullet}$), 2,20-azinobis(3-ethylbenzothiazoline-6-sulfonic acid) diammonium salt (ABTS), and potassium persulfate ($K_2S_2O_8$) were provided by Sigma-Aldrich (St Louis, USA) and used as received without further purification. Granular calcium chloride ($CaCl_2$) was purchased from Merck KGaA (Darmstadt, Germany). Hyaluronic acid sodium salt (MW = 350 000) was purchased from ABCR (Karlsruhe, Germany). Commercial stainless steel (SS) springs ($L = 15.7$ mm, $D = 2.75$ mm) and flat sheets (316L SS, 500 mm × 300 mm × 0.5 mm) were purchased from RS Component (Milan, Italy). Dulbecco's phosphate buffered saline (PBS) and ethanol (≥99.8%) were purchased from

Sigma-Aldrich (St Louis, USA), while deionized water (ddH_2O) was supplied by a Milli-Q Integral purification system (Millipore, Bedford, USA).

2.2 Fabrication of ZR-coated coupons/springs

316L SS sheets were cut into squared pieces with a size of 18 mm × 18 mm (herein referred to as "coupons") to obtain two-dimensional model substrates for the coating deposition. In order to achieve a homogeneous thickness of the zein coating and a hydrophilic substrate surface, the SS springs and coupons were initially ultrasonically cleaned with ethanol and deionized water for 10 minutes to remove impurities and then pretreated with O_2 plasma for 2 minutes at 100 W using a Tucano plasma system (Gambetti Kenologia, Milano, Italy). The rutin-loaded zein (ZR) solution was prepared by dissolving rutin in 5% v/v DMSO and then diluting it with a mixture of ethanol (76% v/v) and deionized water. Afterwards, zein powder was added to form a solution composed of 15% w/v zein and rutin (10% w/w_{zein}), as reported in Table 1. The mixture was stirred at room temperature at a mixing speed of 700 rpm for 60 minutes until complete dissolution.

The cleaned SS springs/coupons were weighted and immediately coated with rutin-loaded zein by means of a dip-coating method, as shown in Fig. 1. Briefly, the previously made zein solution was poured into a 50 mL glass beaker and the substrates were dipped for 10 seconds. Subsequently, the samples were slowly withdrawn from the solution and placed under a fume hood for 12 hours to allow for the evaporation of the residual solvents and to produce a thin, hardened zein film. For the entire drying period, the samples were placed under a fume hood, standing vertically against a wall, in order to achieve a smoother and more homogeneous coating of the polymer. After the coating deposition, the resulting substrates were weighed again. The difference between the two weights compared to the weight of 1 mL of dried ZR solution provides an estimation of the coating volume effectively deposited onto the substrate. This information can be used to determine the quantity (μg) of zein and rutin deposited on each sample, for the following characterizations.

Table 1 Drug-polymer formulations for the bilayer coated stainless steel substrates

Layer	Matrix material	Functional molecule
Active layer (ZR)	Zein 15% w/v in Milli-Q H_2O/ethanol (80 : 20 v/v)	Rutin 10% w/w_{zein}
Sacrificial layer (cAlg)	Alginate 3% w/v in Milli-Q H_2O + $CaCl_2$ 10% w/v in H_2O/ethanol (25 : 75 v/v)	—

2.3 Fabrication of the sacrificial layer onto the coupons/springs

A 3% w/w sodium alginate solution (Alg) was used to deposit a top layer onto the ZR-coated samples. Briefly, alginic acid sodium salt and ddH_2O were mixed at room temperature until complete dissolution. A schematic diagram of the double-layer coating is shown in Fig. 1. ZR-coated samples were dipped in the alginate solution and placed under a fume hood to dry. A 10% w/w $CaCl_2$ ethanolic solution (1.35 M, containing 75% v/v EtOH) was sprayed onto the ZR/Alg-coated surface using an airbrush spray coating system (0.55 mm nozzle diameter, model VL-SET, Paasche Airbrush Company, Chicago, USA) to cross-link the alginate chains with Ca^{2+} ions and partially stabilize the coating. The samples were then dipped into the same calcium chloride solution for additional 15 seconds, in order to obtain a complete cross-linked layer. The resulting samples (ZR/cAlg) were dried overnight at room

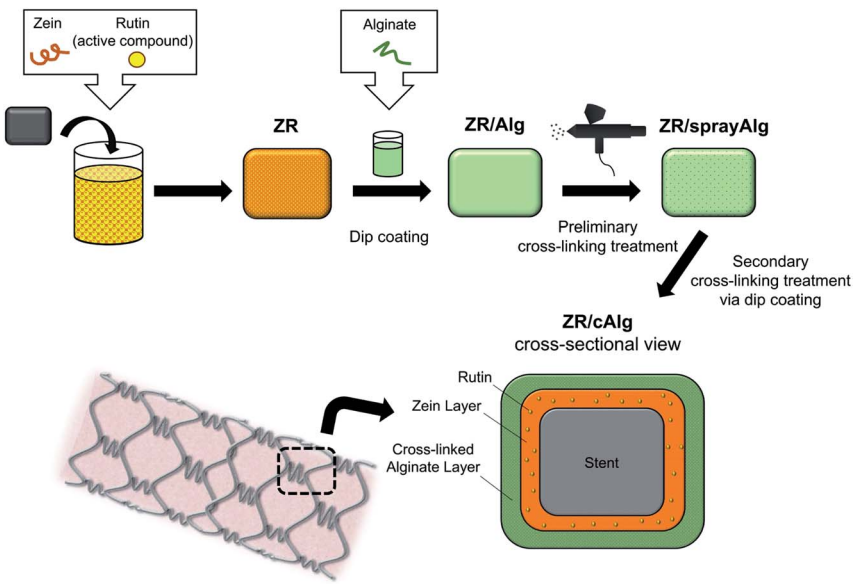

Fig. 1 Schematic illustration of the fabrication process and the cross-sectional final rendering of the bilayer coating on stainless steel substrates (*e.g.* stent).

temperature prior to characterization. Table 1 lists the formulation details used for the complete coating of the substrates.

With the aim of optimizing the sacrificial layer, other materials have been tested in a preliminary phase of the study: a 1% w/v hyaluronic acid (HA) solution in ddH_2O, a 1% w/v hyaluronic acid (HA) solution with 1% w/v poly(ethylene glycol) (PEG) in ddH_2O (HA-PEG) and a 15% w/v zein (Z) solution in 80% v/v EtOH were prepared and applied by a dipping method on ZR-coated samples.

2.4 Surface topography

The morphologies of the coated samples were examined by scanning electron microscopy, using a JSM-6490LA scanning electron microscope (SEM, JEOL Inc., Peabody, USA) at 10 kV accelerating voltage. The specimens were placed on conductive carbon tape, mounted onto SEM stubs, and sputter-coated with a 10 nm layer of gold to improve the electrical conductivity of the surfaces. Digital images of the surface topographies and cross-sections were collected at various magnifications.

Coating thicknesses were measured using a surface profilometer (Ambios XP-2, AmBiosTech, Santa Cruz, USA) equipped with a diamond-tipped stylus. A scratch was applied manually to the flat-coated specimens using a lancet. Subsequently, the stylus tip with a radius of 2 μm moved across the scratched surfaces under a constant load of 0.5 mg with a speed of 0.5 mm s^{-1}. Being a well-recognized technique used to extract topographical data from a surface, the surface profilometer with similar parameters was used to obtain the arithmetic roughness value of each layer.[34] In particular, a straight line of 3 mm was drawn by the stylus tip on each sample and the in-built software XP-2 was used to calculate the arithmetic roughness of the samples across the drawn line.

2.5 Fourier transform infrared spectroscopy

Fourier Transform Infrared (FTIR) spectra of the different substrates were acquired using an infrared spectrometer (Vertex 70 FT-IR Spectrometer, Bruker, Germany). Measurements in the ATR (Attenuated Total Reflection) mode were performed between 4000 and 750 cm^{-1}, using 32 scans at a resolution of 4 cm^{-1}.

2.6 Contact angle measurements

Static contact angle measurements were obtained for the coated coupons using a contact angle goniometer (Dataphysics OCA 20, Filderstadt, Germany) by means of a sessile drop method. Briefly, 5 μL drops of ddH_2O were deposited onto 10 different spots on each sample surface with a micro-syringe. The acquired images were elaborated using the SCA 20 Software (Data Physics Instruments GmbH, Filderstadt, Germany). The angle between the baseline of the drop and the tangent at the drop boundary was determined; the contact angle measurements were calculated by taking the arithmetic average of the left and right contact angles of each droplet.

2.7 Mechanical properties analysis

In order to determine the critical load values, scratching tests were performed with a Micro-Combi Tester (Anton-Paar, Peseux, Switzerland) using a diamond conical indenter with a 0.1 mm diameter. A 5 mm scratch test was performed on the surfaces of the samples, applying a progressive load from 30 to 1000 mN with a speed rate of 5 mm min^{-1}. All mechanical measurements were taken at three different locations on each coating to check the homogeneity of the deposition process.

2.8 X-ray photoelectron spectroscopy

Chemical elements of the coated surfaces within 10 nm in depth were investigated using X-ray photoelectron spectroscopy (XPS) using an electron spectrometer (Lab2, Specs, Berlin, Germany) equipped with a monochromatic X-ray source (set at 1486 eV) and with a hemispherical energy analyzer (Phoibos, HSA3500, Specs, Berlin, Germany). The applied voltage of the Al Kα X-ray source was set at 13 kV and the applied current at 8 mA. The pressure in the analysis chamber was $\sim 1 \times 10^{-9}$ mbar.

2.9 Zein-coated substrates degradation

In order to study the polymer degradation kinetics in PBS buffer, a polymer solution (zein 15% w/v) was prepared in 80% v/v EtOH and used to coat cleaned SS coupons. Briefly, several accurately weighed samples (before and after the zein coating) were placed at the bottom of individual wells in a 6-well plate. Each well was filled with 3 mL of PBS (pH 7.4). The plates were sealed with parafilm and placed in an incubation shaker, where the agitation rate and temperature were maintained constant (75 rpm and 37 °C) for the duration of the experiment, to mimic the physiological environment of the human body. At fixed time points (ranging from 15 minutes to 21 days), the incubation media were completely withdrawn for analysis, and 3 mL of fresh PBS were immediately replenished into each well. Absorbance at 280 nm (zein λ_{max}) was determined with a Cary 6000i UV-Vis-NIR spectrophotometer (Varian, Palo Alto, USA). The amount of zein released from each coupon was calculated by an appropriate calibration curve. The degradation test was carried out in triplicates for each time point and the results were expressed as the percent of cumulative zein degraded as a function of the incubation time according to eqn (1).

$$\text{Cumulative amount of degraded zein (\%)} = \frac{\text{Mass of zein into the medium (at time} = t)}{\text{Total mass of zein (at time} = 0\ )} \times 100 \quad (1)$$

In order to assess the presence of surface morphological changes during the degradation experiment, a reference sample was selected at the end of specific time points, washed with deionized water, and vacuum dried for 24 hours. Morphological features of the degraded coatings, such as pore shape and size, were observed by SEM as previously presented in paragraph 2.4. From such images, a porosity analysis was conducted to check for the mean pore sizes and the pore size distribution curves using an image analysis software (ImageJ, Wayane Rasband, NIH, http://rsbweb.nih.gov/ij/).

2.10 Rutin release studies

The release of rutin from different coated SS coupons (either with one or two layers) was assessed in a similar way to the

methodology previously detailed in paragraph 2.9. Solutions with known amounts of rutin dissolved in PBS were used to prepare a calibration curve, in order to determine the concentration of the active compound released in the incubation media at each time point. Collected media samples were analyzed by UV spectroscopy and the absorbance at 360 nm (rutin λ_{max}) was recorded. Results were expressed as the cumulative percent of rutin released as a function of the incubation time according to eqn (2).

$$\text{Cumulative amount of released rutin (\%)} = \frac{\text{Mass of rutin into the medium (at time} = t)}{\text{Total mass of rutin initially loaded (at time} = 0)} \times 100 \quad (2)$$

The statistical significance was evaluated using one-way ANOVA, followed by Bonferroni's post *hoc* test using Origin 2019b 64Bit. A value of $p < 0.05$ was considered significant.

As previously presented for zein-coated samples, a reference ZR sample was selected at the end of specific time points, washed with deionized water, and vacuum dried for 24 hours. From the SEM images, a porosity analysis was performed to measure mean pore size and to plot pore size distribution curves using an image analysis software, as reported in paragraph 2.9.

2.11 Antioxidant assays

The antioxidant activity of the released samples was determined with the $ABTS^{\bullet+}$ assay according to the method described by Re *et al.* (1999). The $ABTS^{\bullet+}$ radical cation, strongly colored in green, is formed by reacting a 7.0 mM solution of ABTS in water with a 2.45 mM solution of potassium persulfate. The mixture was left for 15–16 hours in the dark until the reaction was complete and the absorbance at 728 nm was stable. For the evaluation of the antioxidant activity, the $ABTS^{\bullet+}$ solution was diluted with deionized water to obtain an absorbance of 1.00 ± 0.02 at 728 nm. At fixed time points, the same used for the rutin release studies, an aliquot of the extracts (150 μL) was mixed with 1850 μL of $ABTS^{\bullet+}$ diluted solution and the absorbance was read after 1 minute by means of a UV-Vis spectrophotometer. The absorbance of a control sample to which 150 μL of PBS had been added was measured in the same way. A rutin stock solution in PBS and its diluted products were used for comparative purposes. The $ABTS^{\bullet+}$ scavenging ability of each sample was determined according to eqn (3):

$$\text{Radical scavenging activity} = \frac{(A_0 - A_1)}{A_0} \times 100 \quad (3)$$

where A_0 is the absorbance of the control radical solution and A_1 is the absorbance of the radical solution after adding the extract containing rutin.

The antioxidant capacity of the released samples was also determined by the $DPPH^{\bullet}$ free radical scavenging method. $DPPH^{\bullet}$ powder was dissolved in ethanol and shaken for 30 minutes under magnetic stirrer agitation, in order to obtain a 0.2 mM solution. Aliquots of 150 μL of the extracted sample solutions and 1 mL of $DPPH^{\bullet}$ solution were mixed in a cuvette and incubated for 30 minutes in the dark at room temperature. Afterwards, the absorption was measured at 522 nm with a UV-Vis spectrophotometer. The absorbance of a control sample, to which 150 μL of PBS had been added, was measured in the same way. A rutin stock solution in PBS and its diluted products were used for comparative purposes. The $DPPH^{\bullet}$ scavenging activity of each sample was determined according to eqn (3).

The statistical significance was evaluated using one-way ANOVA, followed by Bonferroni's post *hoc* test using Origin 2019b 64Bit. A value of $p < 0.05$ was considered significant.

2.12 *In vitro* studies with human umbilical vein endothelial cells

The biocompatibility of glass slides (18 × 18 mm) coated with ZR and ZR/cAlg was firstly assessed on human umbilical vein endothelial (HUVEC, Carlo Erba, Italy) as follow described. Samples were initially subjected to UV-light irradiation for 30 minutes in order to reduce possible initial microbial and environmental contamination. Then, samples were laid onto a 24-well plate (1.9 cm^2), cells were seeded onto each slide at 10×10^5 cells per well seeding density, and were grown for 24 and 48 hours at 37 °C in a humidified 5% CO_2 incubator. Cells cultured in the growth medium were considered as standard control. After 24 and 48 hours of culture, cell viability was tested by means of alamarBlue™ assay (Thermo Fisher, Italy). Based on the manufacturer's instructions, cells were washed once with PBS and treated with DMEM medium without red phenol (Dulbecco's Modification of Eagle's Medium with 4.5 g L^{-1} glucose & amp; sodium pyruvate without L-glutamine, Sigma-Aldrich, Italy) containing 10% v/v alamarBlue™ for 3 hours at 37 °C. The fluorescence intensity was measured at 544 nm excitation and 590 nm emission using a fluorescent microplate reader (FLUOstar Omega Microplate Reader, BMG LabTech, Ortenberg, Germany). Four replicates of each sample were performed, and a one-way ANOVA followed by a post *hoc* Tukey HSD test was employed using Origin 2019b 64Bit as a statistical approach to compare the results. Differences were considered statistically significant at a level of $p < 0.05$.

Furthermore, cells grown for 48 hours onto the samples (ZR- and ZR/cAlg-coated glass slides with $Ø = 13$ mm) were fixed using a 3% v/v glutaraldehyde solution in PBS for 2 hours at room temperature. The substrates were washed three times with PBS and cellular cytoskeletons and nuclei were stained with 150 μL (50 μg mL^{-1}) of Phalloidin-Atto 488 (Sigma-Aldrich, Italy) for 40 minutes in the dark and with 250 μL of Hoechst 33258 (Sigma-Aldrich, Italy) diluted 1 : 10 000 in PBS, for 10 minutes in the dark, respectively. Samples were placed on a microscope slide and imaged using a Confocal Laser Scanning Microscope (CLSM, Leica TCS SP2, Leica Microsystems, Italy) using $\lambda_{ex} = 501$ nm and $\lambda_{em} = 523$ nm for Phalloidin-Atto 488 and $\lambda_{ex} = 346$ nm and $\lambda_{em} = 460$ nm for Hoechst 33258.

2.13 *In vitro* studies with human dermal fibroblasts cells

Adult primary human dermal fibroblasts (HDFa, Thermo Fisher Scientific, Italy) were used as an additional cellular model to investigate the biocompatibility of the fabricated coatings. Cells were cultured in T75 culture flasks in the presence of Medium 106 (under low-serum growth conditions, Thermo Fisher Scientific, Italy), in an incubator at 37 °C and 5% CO_2.

Afterwards, fibroblasts were seeded onto 24-well plates at a density of 7000 cells per cm^2 and let attach overnight. The extraction media from the designed coatings were prepared following the ISO10993-5:2009 standard test specifications. Briefly, the samples (ZR coatings and ZR–cAlg coatings deposited onto 18 × 18 mm glass coverslips) were placed into 35 mm Petri dishes and irradiated under UV light for 20 minutes (10 minutes per side). One mL of culture medium was added into each dish and the wet samples were incubated at 37 °C for 24 hours to obtain the extraction media. The following morning attached HDFa cells were treated with 0.5 mL of the extraction media and incubated for additional 24 or 48 hours, while cells incubated in normal Medium 106 + LSGS (low serum growth supplement) were considered as controls. To determine fibroblasts viability an MTS assay (tetrazolium salt, CellTiter96® AQueous One Solution Cell Proliferation Assay, Promega, USA) was conducted, following the protocol previously established in our group.[35] Statistical analysis was performed by one-way ANOVA with post *hoc* Tukey HSD test. Differences were considered statistically significant at a level of $p < 0.05$.

To visualize the morphology of the cells exposed to the ZR coatings and ZR–cAlg coatings extracts, fibroblasts were plated onto glass coverslips at a density of 5000 cells per cm^2 and treated as above reported. After 48 hours of treatment, cells were washed with pre-warmed PBS (pH 7.4) and fixed with 3.7% paraformaldehyde for 20 minutes. Nuclei were stained with DAPI (Sigma-Aldrich, Italy) incubation (2.5 μg mL^{-1} in PBS) for 15 minutes in the dark. The samples were then permeabilized with 0.3% Triton X-100 for 8 minutes and washed twice with PBS, prior to incubation in Alexa Fluor 488 Phalloidin (Thermo Fisher Scientific, Italy), diluted 1 : 100 in PBS, for 20 minutes in the dark. The coverslips were mounted with Fluoromount-G (Sigma Aldrich, Italy) onto glass slides and imaged under a confocal microscope Nikon A1 (405 nm and 488 nm lasers).

3 Results and discussion

3.1 Fabrication of the bilayer coating on stainless-steel substrates

The ZR/cAlg bilayer coating on SS surfaces was obtained through four steps, as presented in the scheme in Fig. 1. After cleaning with solvents and oxygen plasma, the metal surface was manually dipped in the rutin-loaded zein solution (ZR). In this work, zein served as a polymeric matrix to obtain a drug-eluting coating. With a second step, the 3% alginate solution was applied on the dried ZR surface using the dip-coating method. Afterwards, calcium chloride was applied onto the alginate layer by means of a spray gun system and, subsequently, by dip-coating method, in order to prevent the alginate matrix dissolution and improve the drug retention in the underneath active layer. The presence of calcium ions leads to the formation of cross-linking bonds among the carboxyl groups of guluronic residues belonging to different alginate chains, which then formed a structure having a characteristic arrangement called "egg-box", with calcium ions at the center of it.

In a preliminary phase of this study, a number of commonly used naturally-derived biomaterials, including alginate, zein, hyaluronic acid, with and without PEG, were evaluated as polymers for the construction of the top, sacrificial layer. Among all, alginate was chosen for its non-thrombogenic and hydrophilic nature and for its ability to control drug release when cross-linked. Table 1 lists the formulation details used for the fabrication of the biodegradable bilayer coated SS surfaces.

3.2 Characterization of the zein–rutin (ZR)-coated substrates

Rutin-loaded zein coatings deposited on SS coupons appear homogeneous and smooth both to the naked eye and under the SEM, as can be seen in Fig. 2(a and b). The coated surface of the SS spring, which mimics the curved structure of a stent, resulted uniform, without any cracks (Fig. 2(c and d)).

From the cross-sectional image (Fig. 2(b)), small pores within the ZR film thickness are encountered, probably formed by the fast evaporation of the solvent (ethanol) during the drying phase. The thickness of the ZR layer on SS coupons was examined using a stylus profilometer after the samples were intentionally scratched with a scalpel. The average coating thickness is 6.9 ± 0.8 μm, a value similar to those obtained by analyzing SEM cross-sectional images *via* ImageJ: values of 7.2 μm and 7.1 μm were calculated from Fig. 2(b) and (d), respectively. The measurements with the profilometer, here reported in Table 2 and in Fig. S3(a),† allowed the assessment of the arithmetic roughness of the surface, which was measured to be 219.2 ± 6.8 nm.

The chemistry of the active layer was investigated by ATR-FTIR and XPS. Fig. 2(e) shows the FTIR spectra of zein, rutin, and ZR films, while the full list of absorption peaks with their assignment is provided in Table S1.† Zein spectrum shows four characteristic bands: around 3229 cm^{-1} appears the amide A band corresponding to the stretching of the N–H and O–H bonds of the amino acids of the protein. Another band, called amide I, appears at 1641 cm^{-1}, corresponding to the stretching of the carbonyl (C═O) of amide groups belonging to the peptide bonds. The band at 1533 cm^{-1} is called amide II and derives mainly from in-plane N–H bending and from C–N stretching vibrations in secondary amides. Lastly, the region between 1300 and 1242 cm^{-1} corresponds to the bending and stretching vibrations of the N–H and C–N bonds.[18,36] The symmetrical spectral peak at 1641 cm^{-1} confirms the presence of a higher quantity of α-helices in the secondary structure of zein.[36] In the IR spectrum of rutin, characteristic stretching bands were observed at 1653, 1452 and between 1358 and 1287 cm^{-1} due to C═O, C═C, and C–O bonds, respectively.[37] Distinctive peaks of rutin, especially those representing the aromatic moiety, the C–O and C–O–C bonds of the flavonoid structure, are visible on the right side of the ZR spectrum, thus providing confirmation for the drug incorporation into the protein film. As shown in Fig. 2(e), the two types of polymeric films (zein and rutin-loaded zein) have similar spectra structures, without the appearance of new peaks, indicating that no chemical reactions occurred between the drug and the polymer during the fabrication process. FTIR spectra can also provide information about hydrogen bonding among components in ZR films, as suggested for example from the shifting of the O–H stretching

vibration peak of zein from 3229 to 3283 cm^{-1} after rutin was loaded. From these results, it is clear how the forces including hydrogen bonding, van der Waals forces, and electrostatic forces are responsible for the film structure after solvent evaporation.

XPS was employed to investigate the surface elemental composition of zein and ZR films and the corresponding chemical percentages are summarized in Table S4.† The incorporation of rutin into zein films causes a reduction of nitrogen (N) and oxygen (O) percentages, while the carbon (C) content increases. This result demonstrates the presence of rutin, with its higher carbon content and absence of nitrogen atoms, near the surface of the sample.

A sessile drop method was used to obtain experimental data of the degree of hydrophilicity/hydrophobicity of the prepared ZR-coated SS surfaces. From the literature, it is known that zein has an almost equal amount of hydrophobic and hydrophilic amino acids, which induces their aggregation and self-assembly into films. A value of $61.03 \pm 1.6^{\circ}$ (data not shown) was obtained with water contact angle experiments for the zein-coated coupons, without any active compound inside the polymer. Rutin-loaded zein coatings resulted more hydrophilic, with a reported value of 38.7 ± 2.1, as shown in Table 2. This is due to the exposure of the hydrophilic drug towards the surface of the composite coating, as shown also by XPS, which leads to a reduction in the water contact angle.

The force required to remove the ZR coating from the steel surface was evaluated by a scratch test. An increasing load, from 30 to 1000 mN, was applied to define the critical load value, which was found to be 321.8 ± 50.2 mN, as reported in Table 2 and in Fig. S3(c).† Reaching this value, the coating completely delaminates from the metal substrate, as shown in Fig. S3(e).† The higher the critical load, the more the coating can be considered scratch-resistant and adhesive to the substrate. Few data in the literature are currently available about the adhesion strength of polymeric coatings on SS stents. Compared with the value obtained from a chitosan–silica coating (52.0 mN), the critical load is dramatically higher in our ZR-coated samples, while a smaller difference is observed when comparing PDLLA and ZR coatings, taking into account that these adhesion tests were performed on different substrates (cobalt-chromium and SS).[38,39] We believe that the adhesion strength between our ZR coating and the SS substrate is sufficient for an optimal design of drug-eluting stents.

3.3 Degradation and release profiles of rutin from zein–rutin (ZR)-coated substrates

Zein-coated SS coupons were incubated in PBS buffer over a period of 21 days. A first degradation study of the samples coated with a drug-free polymer was carried out to assess the matrix response in a water-like environment. Fig. 3(a) presents the results of the polymer degradation kinetic study, which appears biphasic with an initial rapid degradation over the first 3–4 days, followed by a slower but steady rate of degradation for the next 20 days. The amount of zein degraded was determined according to eqn (1). Within 21 days, the samples released approximately 55% of the zein polymer mass initially deposited on each coupon, which suggests a high stability of the protein coating in water-based solutions. Afterwards, zein was examined as a potential drug-encapsulating polymer. The release of rutin from the ZR coatings was carried out as described in Section 2.10. Fig. 3(b) reports the release profile of rutin from

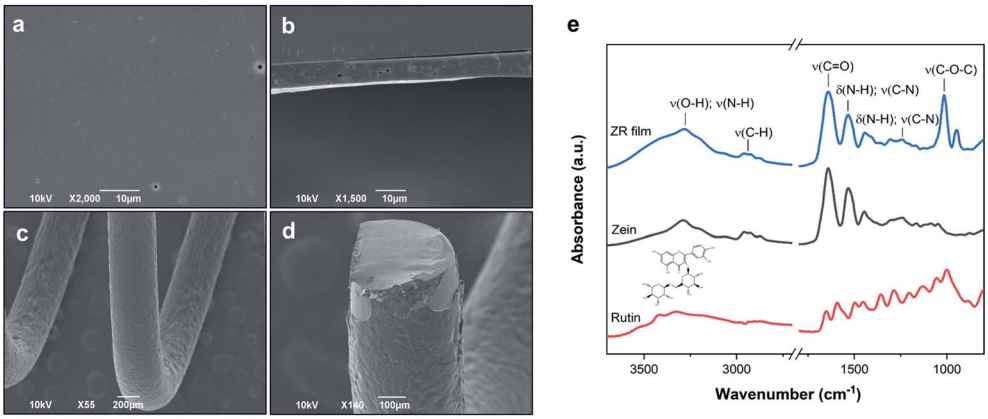

Table 2

Coating material	Water contact angle (°)	Critical load (mN)	Coating thickness (μm)	Arithmetic roughness (nm)
Rutin-loaded zein (ZR)	38.7 ± 2.1	321.8 ± 50.2	6.9 ± 0.8	219.2 ± 6.8

Fig. 2 Physico-chemical characterization of the active layer. SEM micrographs of the rutin-loaded zein coatings: surface and cross-sectional views of a stainless steel-coated coupon (a, b) and spring (c, d). FTIR spectra of rutin powder, zein, and rutin-loaded zein (ZR) films, with insert showing the rutin chemical structure (ChemDraw) (e). Table 2 reports the physico-chemical properties of the rutin-loaded zein coating deposited onto a stainless-steel coupon, using static sessile drop method, stylus profilometer, and scratch tests.

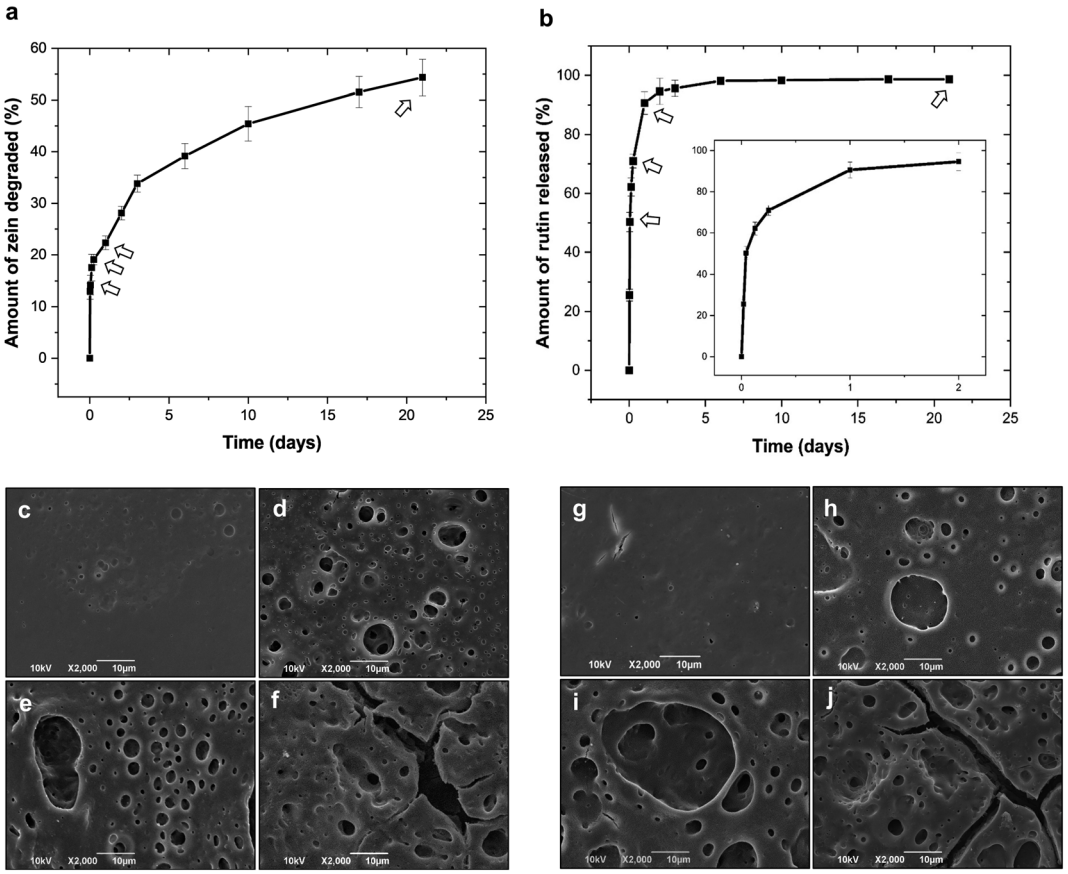

Fig. 3 Degradation, morphologies, and rutin release behaviours of rutin-loaded zein coatings. Cumulative zein matrix degradation (a) and rutin release profile (b) from the ZR coating, with an inset highlighting the release kinetics between 0 and 2 days. The arrows in the graphs identify the time points at which selected samples were taken in order to be analyzed under the microscope. SEM images of zein and ZR coatings after different incubation times: 1 hour (c, g), 6 hours (d, h), 24 hours (e, i), and 21 days (f, j). Pitting, craters and cracks are more visible with time.

the ZR-coated coupons obtained as the cumulative percentage of the drug released as a function of time, according to eqn (2). The release profile suggests that rutin elution from ZR coatings initially occurs due to the matrix surface erosion and to the subsequent release of the hydrophilic drug entrapped near the outer surface of the film. This burst effect during the first 24 hours is followed by a diffusional-degradation controlled phase as a consequence of hydrolysis and penetration of water molecules inside the zein matrix, up to the end of the experiment. In fact, it has been previously demonstrated that degradation of proteins in aqueous media is primarily due to the hydrolysis of the peptide bonds in the backbone of the macromolecules.[3] In our system, approximately 90.6% of the drug is released within the first 24 hours and a cumulative release of 98.7% occurred over a period of 21 days. Zein shows a faster biodegradability when compared to synthetic biodegradable polymers, such as poly(glycolic acid), PLGA, PLLA, and polycaprolactone, which exhibit degradation times of at least 1.5, 2, 6, and 24 months, respectively.[40] For example, Pan *et al.* reported a 60% mass loss for PLGA coating films after 3 months in PBS, and around 70% of the curcumin loaded on the stents was released after 18 days of incubation.[41] Slow, yet incomplete, releases of hydrophobic drugs, such as curcumin, paclitaxel, and sirolimus (SRL), from synthetic biodegradable polymers are often reported in the literature. Kim *et al.* studied the release kinetics of SRL from PLGA-coated stents, which show an initial burst release (around 51% within 2 days) and 69% of the drug released after 28 days.[42] Similarly, Bedair *et al.* noticed an initial burst release of SRL from PDLLA-coated substrates and the complete detachment of the coated layer after 28 days of incubation in PBS.[39]

However, these initial burst releases are not preferable in DES, especially when using potentially toxic compounds such as SRL. As far as for materials of natural origins, polymers derived from bacteria, such as poly(3-hydroxyoctanoate) and poly(3-hydroxybutyrate), have been studied as blend films, showing 97% of aspirin released within a period of 25 days, however, such a slow drug-release rate is observed only when the drug lies within the crystalline regions of the polymers.[43] In a different study, ethanol-treated silk-fibroin films showed a slow but incomplete SRL release (41% after one day and 64% at 14 days).[11] The results obtained from our system, ZR single layer, are in accordance with the previous literature on drug-eluting zein matrices.[27,28,44]

Morphological changes during degradation and drug release studies were investigated using SEM, after rinsing the samples in deionized water, as described in paragraph 2.9. SEM images of the degraded coatings fabricated with zein and ZR are shown in Fig. 3(c–f) and Fig. 3(g–j), respectively.

Although macroscopically both coatings appeared intact even after several days of exposure to the aqueous media, SEM images revealed a degree of surface erosion starting from the first few hours. From this analysis, it was possible to establish that the hydrolysis of the polymer tends to occur uniformly across the matrix. The first signs of coatings degradation are small pores with average diameters of 1.9 and 2.1 μm, developing on the surfaces of zein and ZR films after a short period of PBS incubation (6 hours). For longer experimental times, the samples show deeper and larger degradation pores and craters, with their mean diameters increasing (up to 35 μm) and their distributions becoming denser. Analysis of the pore dimensions at different time points is reported in Fig. S1 and Table S2.† Interestingly, over time, pores tend to connect together to form larger pore structures and cracks on the surface, as clearly revealed by Fig. 3(f and j). The obtained results are promising for a successful fabrication of a safe DES, since marketed devices are usually coated with synthetic polymers that do not fully degrade after releasing their carrier, thus causing adverse side effects.

3.4 Characterization of the bilayer coating

Cross-linked alginate as a sacrificial layer was added on top of the ZR active coating in order to protect the underneath layer from light and moisture and to fine-tune the drug release rate. The surface morphologies and cross-sectional microstructures of the resulting ZR/cAlg bilayer coating on the SS substrates were investigated using SEM, as shown in Fig. 4(a–f). The images reveal a homogeneous coating with minimal structural defects, which is essential to ensure uniform drug delivery and device biocompatibility. Fig. 4(f) shows a SEM micrograph of the coated spring after being chopped with shears. As a consequence of this cut, a slight delamination of the coating from the substrate is observed, making even more visible the bilayer structure along the coated spring. Using a stylus profilometer, the thickness of the scratched ZR/cAlg coating was determined to be 15.4 ± 0.7 μm, as presented in Table 3 and in Fig. S3(b).† This result is in agreement with the mean value of 14.9 μm measured from the SEM cross-sectional micrographs (Fig. 4(b and f)) with an image analysis software. In a parallel experiment, other natural polymers were tested as sacrificial layers, such as zein and hyaluronic acid, with and without PEG. The formation of bilayer films obtained *via* dip-coating method onto previously deposited ZR-coated samples is confirmed by SEM cross-sectional images, as reported in Fig. S2(b–d).† The average

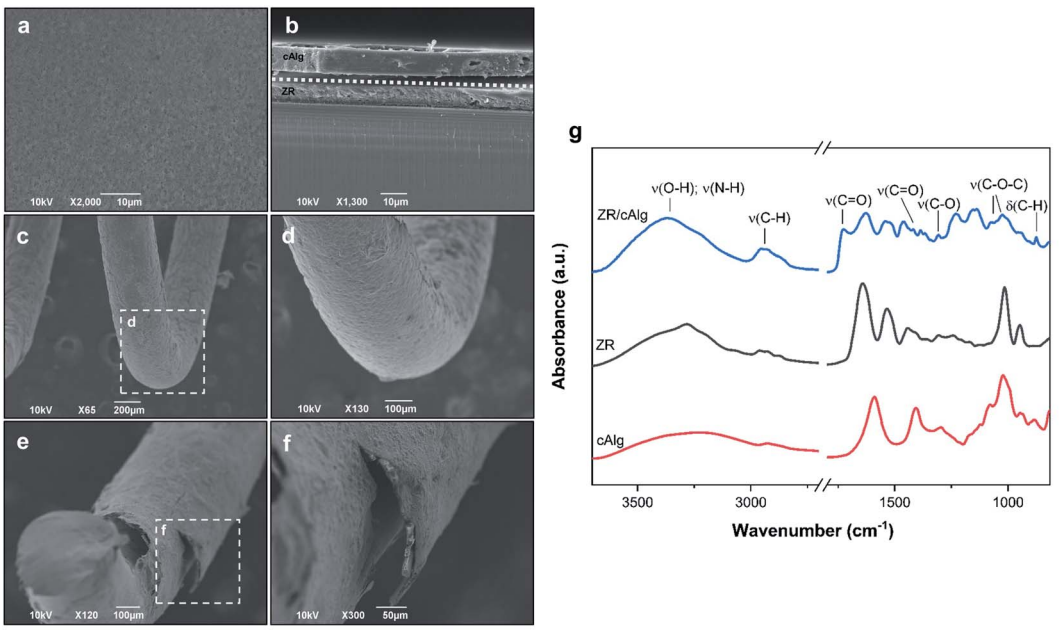

Table 3

Coating material	Water contact angle (°)	Critical load (mN)	Coating thickness (μm)	Arithmetic roughness (nm)
ZR/cAlg bilayer (Cross-linked alginate + rutin-loaded zein)	25.9 ± 3.7	768.3 ± 122.7	15.4 ± 0.7	749.9 ± 42.6

Fig. 4 Physico-chemical characterization of the ZR/cAlg bilayer coating. SEM micrographs of ZR/cAlg coatings: surface and cross-sectional views of a stainless steel-coated coupon (a, b) and spring (c, e). Magnifications of the spring coating morphology are depicted in (d, f). The dotted line in (b) delimits the separation between the two layers. FTIR spectra of ZR, cross-linked alginate, and ZR/cAlg films (g). Table 3 reports the physico-chemical properties of the ZR/cAlg bilayer coating deposited onto a stainless-steel coupon, using static sessile drop method, stylus profilometer, and scratch tests.

thicknesses of the different sacrificial layers were also measured (Table S5†). Between the tested materials, cross-linked alginate was chosen for further characterization studies, due to its good adhesion to the underneath protein film and its hydrophilicity. Moreover, compared to other polymers such as hyaluronic acid, the addition of cross-linked alginate as a sacrificial layer allows a slower drug release rate from the underneath ZR layer coating, as shown in Fig. S2(a) and Table S5.†

ATR-FTIR spectroscopy was performed to analyze the chemical content and the possible interactions between the ZR and cross-linked alginate layers. Listed in Table S3† are the absorption bands associated with the samples under study. The spectrum of cross-linked alginate presented in Fig. 4(g) highlights the presence of four main bands at 3227, 1589, 1406, and 1022 cm^{-1} that can be attributed to O–H vibrations, asymmetric and symmetric C–O–O^- vibrations, and C–O–C vibrations of glycosidic bonds, respectively. In the ZR/cAlg FTIR spectrum, the amide I band at 1641 cm^{-1} appears to be overlapped with the characteristic alginate band at 1589 cm^{-1}, being now observed at 1636 cm^{-1} as a single asymmetric band.[44] Small peaks shifting to lower wavenumbers can be a consequence of possible ionic interactions, for example between the alginate carboxylate groups with calcium ions or protonated zein amino groups.[45,46] The band corresponding to vibrations of the amide II groups occurs at 1518 cm^{-1} in the bilayer spectrum, confirming the existence of interactions between the protein and the polysaccharide. A new band at 1732 cm^{-1} is observed, corresponding to the asymmetric stretching of C=O bonds in some protonated carboxylic acid groups of alginate, which appears after washing the ZR/cAlg samples with deionized water.[45]

XPS analysis was performed to characterize the surface chemical composition of the samples at a 10 nm depth from their surface (results are reported in Table S4†). Considering the use of sodium alginate in the fabrication of the sacrificial layer, the main elements found on the surface of the ZR/Alg samples were carbon and oxygen with a percentage of 71.4 and 23.8%, respectively, with a small amount of sodium (Na) and calcium (Ca) ions (1.4 and 0.5%). The high percentage of calcium in the ZR/cAlg samples confirms the successful cross-linking process. Moreover, the ratio between calcium and chlorine is around 1 : 2 (Ca^{2+} : Cl_2^-), which is consistent with the $CaCl_2$ chemical formula.

Following the application of the alginate layer and the use of calcium chloride on the ZR-coated metallic coupons, a marked reduction of the water contact angle was observed, as it dropped from 38.7 ± 2.1° to 25.9 ± 3.7°. The surface resulted very hydrophilic, in agreement with the data in the literature. Surface hydrophilicity will positively influence the biocompatibility of coated metal substrates by causing a decrease in the number of adsorbed platelets and proteins.[16,47] Surprisingly, even if the samples were uniformly coated with the cross-linked alginate layer, the surface roughness of the ZR/cAlg coatings increased (749.9 ± 42.6 nm) when compared to ZR/Alg (559.4 ± 18.1 nm, data not shown) and ZR coatings (219.2 ± 6.8 nm), as reported in Table 3. This can be explained by the existence of Ca^{2+} in the "egg-box" structure formed by the interactions between alginate and calcium ions. Roughness and small irregularities of the film surface tend to increase when cross-linking occurs.[46] Lastly, the adhesion stability of the ZR/cAlg bilayer coating with a stainless-steel substrate was quantitatively evaluated by a scratch test. The critical load was determined from the scratch profile of the load-displacement graph, reported in Fig. S3(d),† and it was verified with the corresponding optical image of the scratch track, shown in Fig. S3(f).† The average critical load value was found to be 768.3 mN, demonstrating a strong adhesion between our fabricated coating and the SS substrate, which is ideal for the design of a DES.

3.5 Release profile of rutin from the bilayer coating

The cumulative release percentages of rutin from single layer ZR, bilayer ZR/sprayAlg and ZR/cAlg coatings on SS coupons were monitored over 21 days and the results are reported in Fig. 5(a). The rate of drug release from zein films is controlled and sustained by adding on top the sacrificial layer and by treating the upper alginate matrix with a suitable amount of

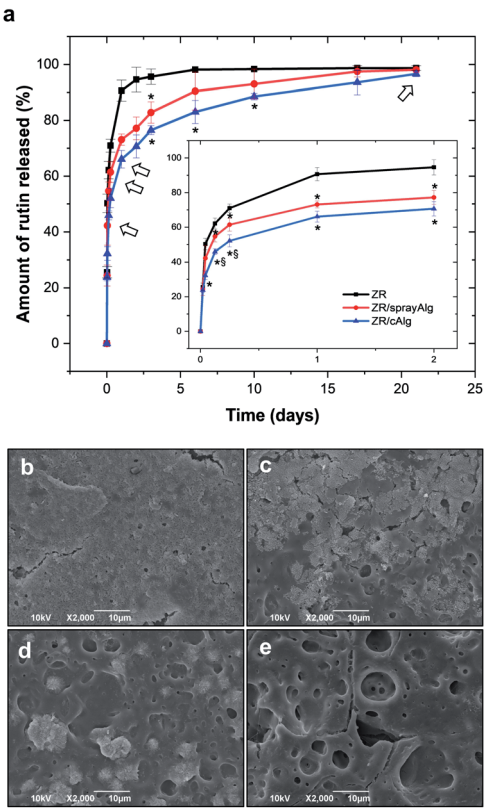

Fig. 5 Morphologies and rutin release behaviors from bilayer coatings presenting alginate as the sacrificial layer. Cumulative release profiles of rutin from ZR (black line), ZR/sprayAlg (red line), and ZR/cAlg (blue line) coatings (a), with an inset highlighting the release kinetics between 0 and 2 days. The arrows in the graphs identify the time points at which selected samples were taken in order to be analyzed under the microscope. SEM images of ZR/cAlg coatings after different incubation times: 1 hour (b), 6 hours (c), 24 hours (d), and 21 days (e). A significance of $p < 0.05$ (* for ZR/sprayAlg or ZR/cAlg and ZR and § for ZR/sprayAlg and ZR/cAlg) was considered.

$CaCl_2$, acting as a hardening agent. Both the samples coated with alginate, either employing one or two steps of cross-linking, exhibit a slower rutin releasing profile. Furthermore, the drug elution from these bilayer samples exhibits a reduced initial burst release.

After 24 hours of incubation in PBS, the ZR/cAlg and ZR/sprayAlg samples showed 66.1 ± 3.2% and 73.1 ± 2.0% of drug released, respectively. Both values are indeed lower than those obtained from the ZR samples (90.6 ± 3.2% of drug release, Fig. 3(b)). The second step of cross-linking is needed in order to achieve a complete coverage of the ZR underlying film by a fully cross-linked alginate layer.

Compared to double-layer biodegradable synthetic coatings, our designed ZR/cAlg bilayer shows better results in terms of drug release. For example, Huang *et al.* used PLGA to fabricate both inner and top layers and reported a burst release of triflusal (a hydrophilic drug) of 60% on the first day with almost 100% release by day 5.[48] From a complex blend of PLLA, PLGA, and PVP, with an additional PVP top layer, SRL release was observed for 48 days by Thakkar and co-workers, with almost all the drug being released within 5 days.[49] ZR/cAlg bilayer exhibits a more gradual drug-release rate also when compared with naturally derived coatings. As an example, Chen *et al.* fabricated multi-layers of cross-linked collagen and reported a 90% of SRL release within 4 days.[10]

Being a hydrophilic material, both bulk and surface erosion of the alginate matrix takes place at a rapid rate. Surface morphologies of the degraded ZR/cAlg-coated samples at different time points were captured by SEM and are reported in Fig. 5(b–e). Small pieces of the cross-linked alginate layer delaminating from the coating are visible during the first 24 hours, while at the same time the degradation of the underlying ZR layer is confirmed by the appearance of small pores. The presence of the sacrificial layer delays the formation of these pores, compared to what observed for zein and ZR single layers in Fig. 3(b–e) and (g–j).

3.6 Antioxidant properties of the fabricated coatings

As presented in the previous section, the aqueous extracts from ZR and ZR/cAlg coatings were found to contain considerable amounts of released rutin, which is known to be a strong antioxidant compound. The measured free radical scavenging activities (RSA) of the samples extracted from the coatings at

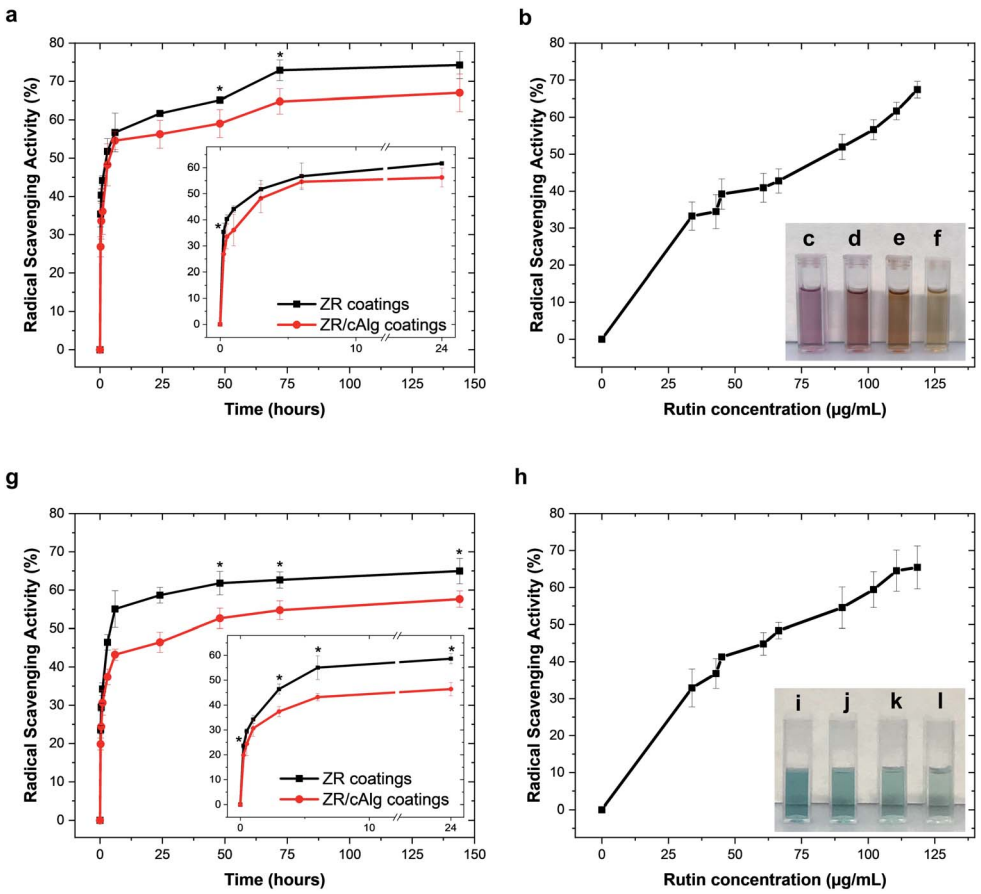

Fig. 6 Antioxidant activity of the released active molecule. Radical scavenging activity (RSA) against DPPH$^{\bullet}$ (a) and ABTS$^{\bullet+}$ (g) free radicals of PBS extracts from ZR coatings (black lines) and ZR/cAlg coatings (red lines), with insets highlighting the RSA between 0 and 24 hours. The calibration curves (b and h) were obtained with rutin-containing solutions at different concentrations (from 33.8 to 118.5 μg mL^{-1}). The insets in (b) and (h) show the colour change of the scavenging solutions at room temperature in the presence of 0 μg mL^{-1} (c and i), 33.8 μg mL^{-1} (d and j), 45 μg mL^{-1} (e and k) and 118.5 μg mL^{-1} (f and l) of rutin. A significance of $p < 0.05$ (*) was considered.

determined time points for up to 144 hours against DPPH$^{\bullet}$ and ABTS$^{\bullet+}$ radicals are shown in Fig. 6(a) and (g), respectively. The extracts containing rutin were more effective in scavenging DPPH$^{\bullet}$ than ABTS$^{\bullet+}$ radicals. After 144 hours, the RSA against DPPH$^{\bullet}$ and ABTS$^{\bullet+}$ free radicals reached 74.3 ± 3.5% and 65.0 ± 3.3% with ZR extracts, and 67.0 ± 4.9% and 57.7 ± 2.1% with ZR/cAlg extracts, respectively. The differences between the two assays might be due to the fact that the chemical properties and complexity of the extracted samples could lead to varying bioactivity results depending on the method adopted. Both assays are based on the hydrogen donating ability of the radicals and involve the reduction of a coloured molecule, however, the DPPH$^{\bullet}$ assay is conventionally conducted in ethanol or methanol, while the ABTS$^{\bullet+}$ assay is carried out in aqueous media. Factors such as stereo-selectivity of radicals or solubility of flavonoids have also been reported to affect the ability of antioxidant compounds to quench different radicals in different testing systems.[50] For comparison, Fig. 6(b) and (h) show the scavenging activity against DPPH$^{\bullet}$ and ABTS$^{\bullet+}$ free radicals as a function of rutin concentration, and similar trends can be observed. As expected, it is evident that both RSA increase with increasing concentration of rutin (this pattern is called "dose-dependent antioxidant activity"). Both the antioxidant assays show how rutin retains its biological activity during the fabrication process and the subsequent release test in aqueous media, over an extended period of time.

3.7 Cell biocompatibility of the fabricated coatings

Endothelial cells and fibroblasts are involved both in the healing process and in the maintenance of the cardiovascular system physiology and, as known, endothelial cells form a lining of the vascular wall and therefore play a key role in retaining the vascular homeostasis.[8] Based on the potential application of the coatings in drug-eluting stent production and considering these premises, it is crucial to demonstrate their compatibility on both cell lines. Here the biocompatibility and the cell adhesion results are reported while the results with fibroblasts are shown in Fig. S4.† As reported in Fig. 7(a), the designed coatings showed good biocompatibility compared to the standard control. In particular, cells grew up to 86.2% and 100.5% after 24 and 48 hours on ZR-coated substrates, and up to 113.4% and 92.7% after 24 and 48 hours on ZR/cAlg-coated substrates, considering 100.0% the growth on the control. Moreover, no statistical differences between the control and the cells grown on the ZR or ZR/cAlg layers were detected. HUVEC adhesion after 48 hours of culture on ZR and ZR/cAlg coatings is also reported in Fig. 7(b–d). The zein autofluorescence signal is visible in the blue channel for both samples, thus partially hiding the cell nuclei staining. As shown in Fig. 7(c and d), cell adhesion occurs on both samples,

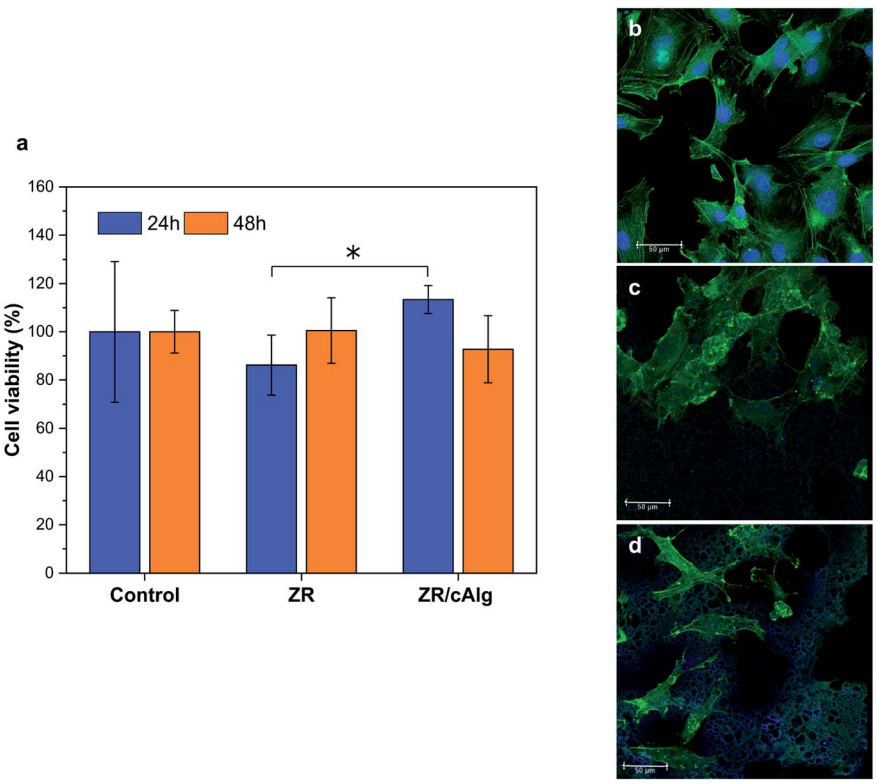

Fig. 7 HUVEC biocompatibility. HUVEC viability (a) evaluated *via* alamarBlue™ assay for cells grown onto ZR and ZR/cAlg coated glass coverslips and under standard conditions (control, uncoated glass coverslips), for 24 and 48 hours; data are shown as mean values ± SD (*$p < 0.05$). CLSM of HUVEC: cells were grown onto a control glass slide (b) or onto glass coverslips coated with ZR (c) and ZR/cAlg (d) for 48 hours before the imaging analysis (scale bar 50 μm). Nuclei are marked with Hoechst 33582 (blue) and cytoskeletons with Phalloidin FITC (green).

confirming that the coated substrates supported the HUVEC growth without impairing their proliferation. In particular, cells grown onto ZR layers appeared polygonal with a cobblestone-shape but clustered, while cells grown onto ZR/cAlg coated glasses became elongated with a spindle-shaped morphology. The morphological response and variations of cells cultured on ZR and ZR/cAlg was partially caused by the surface changes exploited by the natural degradation of the coatings, which led to an unsteady growing surface.

This result is supported by the degradation studies performed in PSB, largely explained in paragraphs 3.3 and 3.5, and reported in Fig. 3(a) and 5(a). Considering both viability data and CLSM analysis, ZR and ZR/cAlg layers demonstrated to be biocompatible materials with no evident cytotoxic effect.

4 Conclusions

In this work, a novel, biodegradable bilayer coating for drug-eluting stents was proposed. In particular, zein in the form of thin films was evaluated for its potential as a carrier matrix for drug-delivery applications, showing slow biodegradability. Rutin release from ZR and bilayer systems was investigated with the goal of evaluating the drug-eluting capabilities of our plant-based polymeric multifunctional coatings. Among the studied polymers, cross-linked alginate resulted to be the best sacrificial covering layer, due to its good adhesion to the underneath protein film and its hydrophilicity. Moreover, when cross-linked, alginate succeeded in delaying the delivery profile of the entrapped antioxidant drug and ensured the biocompatibility of the coated metal substrate. ZR/cAlg layers were successfully fabricated and uniformly coated onto SS substrates by fast and cost-effective dip and spray coating methods. After investigating their physico-chemical properties, the applicability of these coatings for stents was established by evaluating the attachment and proliferation of endothelial cells and fibroblasts. Biocompatibility studies proved the suitability of the developed multi-layered coatings. This should be an interfacial biomaterial capable of creating a pro-healing stent surface that promotes the endothelialization of the device and simultaneously should prevent the adhesion and thrombus formation, typical of platelet interactions.[51]

In conclusion, our designed plant-based bilayer fulfils the key requirements for a successful drug-eluting coating for DES, presenting good physico-chemical properties, drug stability, excellent biocompatibility towards vascular cells, and the ability to carefully control the elution of the drug over 21 days. Our study sets the premises for a new generation of bio-based multilayer DES and dual-drug eluting stent (for multiple drugs and sequential release purposes) that could be developed in the near future, with the aim of improving the cyto- and hemocompatibility of the coating materials, while precisely modulating the drug release kinetics.

Author contributions

Martina Lenzuni: conceptualization, investigation, visualization, validation, writing – original draft. Giulia Suarato: conceptualization, investigation, validation, project administration, writing – review & editing. Dalila Miele: investigation, validation, writing – review & editing. Riccardo Carzino: investigation, validation. Marco Ruggeri: investigation, validation, writing – review & editing. Giuseppina Sandri: validation, supervision, writing – review & editing. Rosalia Bertorelli: conceptualization, writing – review & editing. Athanassia Athanassiou: conceptualization, project administration, supervision, writing – review & editing.

Conflicts of interest

There are no conflicts to declare.

Acknowledgements

We would like to thank Dr Luca Ceseracciu and Dr Marco Salerno, Materials Characterization Facility, Istituto Italiano di Tecnologia, for assistance in performing mechanical tests.

References

1 S. Tadayon, K. Wickramasinghe and N. Townsend, *Popul. Health Metr.*, 2019, **17**, 1–15.
2 D. Buccheri, D. Piraino, G. Andolina and B. Cortese, *J. Thorac. Dis.*, 2016, **8**, 1150–1162.
3 C. Alvarez-Lorenzo and A. Concheiro, *Chem. Commun.*, 2014, **50**, 7743–7765.
4 R. Virmani, G. Guagliumi, A. Farb, G. Musumeci, N. Grieco, T. Motta, L. Mihalcsik, M. Tespili, O. Valsecchi and F. D. Kolodgie, *Circulation*, 2004, **109**, 701–705.
5 P. Roopmani, S. Sethuraman, S. Satheesh and U. Maheswari Krishnan, *RSC Adv.*, 2016, **6**, 2835–2853.
6 T. Palmerini, G. Biondi-Zoccai, D. della Riva, A. Mariani, M. Sabaté, P. C. Smits, C. Kaiser, F. D'Ascenzo, G. Frati, M. Mancone, P. Genereux and G. W. Stone, *J. Am. Coll. Cardiol.*, 2014, **63**, 299–307.
7 C. M. Agrawal and K. A. Athanasiou, *J. Biomed. Mater. Res.*, 1997, **38**, 105–114.
8 A. Strohbach and R. Busch, *Int. J. Polym. Sci.*, 2015, **2015**, 1–11.
9 A. Balaji, S. K. Jaganathan, M. v. Vellayappan, A. A. John, A. P. Subramanian, M. SelvaKumar, H. Mohandas, M. Sundar Raj and E. Supriyanto, *RSC Adv.*, 2015, **5**, 69660–69679.
10 M. C. Chen, H. F. Liang, Y. L. Chiu, Y. Chang, H. J. Wei and H. W. Sung, *J. Controlled Release*, 2005, **108**, 178–189.
11 W. Xu, K. Yagoshi, T. Asakura, M. Sasaki and T. Niidome, *ACS Appl. Bio Mater.*, 2020, **3**, 531–538.
12 F. Wu, J. Li, K. Zhang, Z. He, P. Yang, D. Zou and N. Huang, *ACS Appl. Mater. Interfaces*, 2016, **8**, 109–121.
13 S. Meng, Z. Liu, L. Shen, Z. Guo, L. L. Chou, W. Zhong, Q. Du and J. Ge, *Biomaterials*, 2009, **30**, 2276–2283.
14 Y. Chen, L. Wu, P. Li, X. Hao, X. Yang, G. Xi, W. Liu, Y. Feng, H. He and C. Shi, *Macromol. Biosci.*, 2020, **20**, 1900370.
15 R. Song, M. Murphy, C. Li, K. Ting, C. Soo and Z. Zheng, *Drug Des., Dev. Ther.*, 2018, **12**, 3117–3145.

16 T. Yoshioka, K. Tsuru, S. Hayakawa and A. Osaka, *Biomaterials*, 2003, **24**, 2889–2894.
17 S. Iravani and R. S. Varma, *Green Chem.*, 2019, **21**, 4839–4867.
18 E. Corradini, P. S. Curti, A. B. Meniqueti, A. F. Martins, A. F. Rubira, E. Curti Muniz and C. J. Schaschke, *Int. J. Mol. Sci.*, 2014, **15**, 22438–224470.
19 İ. Arcan, D. Boyacı and A. Yemenicioğlu, in *Reference Module in Food Science*, Elsevier, 2017.
20 R. Shukla and M. Cheryan, *Ind. Crops Prod.*, 2001, **13**, 171–192.
21 H. Xu, Q. Jiang, N. Reddy and Y. Yang, *J. Mater. Chem.*, 2011, **21**, 18227–18235.
22 S. Zhang and Y. Han, *PLoS One*, 2018, **13**, e0194951.
23 Q. S. Sun, J. Dong, Z. X. Lin, B. Yang and J. Y. Wang, *Biopolymers*, 2005, **78**, 268–274.
24 H. J. Wang, Z. X. Lin, X. M. Liu, S. Y. Sheng and J. Y. Wang, *J. Controlled Release*, 2005, **105**, 120–131.
25 J. Fernández-Carneado, M. J. Kogan, S. Castel and E. Giralt, *Angew. Chem., Int. Ed.*, 2004, **43**, 1811–1814.
26 F. Fiorentini, G. Suarato, P. Grisoli, A. Zych, R. Bertorelli and A. Athanassiou, *Eur. Polym. J.*, 2021, **150**, 110414.
27 D. Brahatheeswaran, A. Mathew, R. G. Aswathy, Y. Nagaoka, K. Venugopal, Y. Yoshida, T. Maekawa and D. Sakthikumar, *Biomed. Mater.*, 2012, **7**, 045001.
28 N. Bidyarani and U. Kumar, *RSC Adv.*, 2019, **9**, 40819–40826.
29 K. A. Youdim and J. A. Joseph, *Free Radicals Biol. Med.*, 2001, **30**, 583–594.
30 B. W. Nileeka Balasuriya, H. P. V. Rupasinghe and H. P. Vasantha Rupasinghe, *Funct. Foods Health Dis.*, 2011, **1**, 172–188.
31 T. Kauss, D. Moynet, J. Rambert, A. Al-Kharrat, S. Brajot, D. Thiolat, R. Ennemany, F. Fawaz and M. Djavad Mossalayi, *Arthritis Res. Ther.*, 2008, **10**, 19–28.
32 C. H. Lescano, F. Freitas de Lima, C. A. L. Cardoso, S. C. H. Vieira, F. Z. Mónica and I. Pires de Oliveira, *Food Funct.*, 2021, **12**, 802–814.
33 A. Ugusman, Z. Zakaria, K. H. Chua, N. A. Megat, M. Nordin and Z. A. Mahdy, *Sci. World J.*, 2014, **2014**, 1–9.
34 F. Shady, *ACS Appl. Mater. Interfaces*, 2018, **10**, 9010–9022.
35 G. Suarato, M. Contardi, G. Perotto, J. A. Heredia-Guerrero, F. Fiorentini, L. Ceseracciu, C. Pignatelli, D. Debellis, R. Bertorelli and A. Athanassiou, *Mater. Sci. Eng., C*, 2020, **116**, 111151.
36 L. A. Forato, R. Bernardes-Filho and L. A. Colnago, *Anal. Biochem.*, 1998, **259**, 136–141.
37 O. Abbas, G. Compère, Y. Larondelle, D. Pompeu, H. Rogez and V. Baeten, *Vib. Spectrosc.*, 2017, **92**, 111–118.
38 T. S. Jang, K. H. Cheon, J. H. Ahn, E. H. Song, H. E. Kim and H. do Jung, *Colloids Surf., B*, 2019, **179**, 405–413.
39 T. M. Bedair, Y. Cho, T. J. Kim, Y. D. Kim, B. J. Park, Y. K. Joung and D. K. Han, *Langmuir*, 2014, **30**, 8020–8027.
40 K. J. Jem and B. Tan, *Adv. Ind. Eng. Polym. Res.*, 2020, **3**, 60–70.
41 C. J. Pan, J. J. Tang, Y. J. Weng, J. Wang and N. Huang, *J. Controlled Release*, 2006, **116**, 42–49.
42 J. H. Kim, N. R. Ko, B. Y. Jung and I. K. Kwon, *Macromol. Res.*, 2016, **24**, 931–939.
43 P. Basnett, K. Y. Ching, M. Stolz, J. C. Knowles, A. R. Boccaccini, C. Smith, I. C. Locke and I. Roy, *Bioinspired, Biomimetic Nanobiomater.*, 2013, **2**, 141–153.
44 A. C. S. Alcântara, P. Aranda, M. Darder and E. Ruiz-Hitzky, *J. Mater. Chem.*, 2010, **20**, 9495–9504.
45 G. Lawrie, I. Keen, B. Drew, A. Chandler-Temple, L. Rintoul, P. Fredericks and L. Grøndahl, *Biomacromolecules*, 2007, **8**, 2533–2541.
46 M. J. Costa, A. M. Marques, L. M. Pastrana, J. A. Teixeira, S. M. Sillankorva and M. A. Cerqueira, *Food Hydrocolloids*, 2018, **81**, 442–448.
47 P. Thevenot, W. Hu and L. Tang, *Curr. Top. Med. Chem.*, 2008, **8**, 270–280.
48 Y. Huang, S. S. Venkatraman, S. Subbu, F. Y. C. Boey, E. M. Lahti, P. R. Umashankar, M. Mohanty, S. Arumugam, L. Khanolkar and S. Vaishnav, *Biomaterials*, 2010, **31**, 4382–4391.
49 A. Thakkar, A. Raval, R. Mandal, S. Parmar, A. Jariwala, J. Tailor and A. Mehta, *J. Med. Devices*, 2013, **7**, 011005.
50 S. O. Okoh, O. T. Asekun, O. B. Familoni and A. J. Afolayan, *Antioxidants*, 2014, **3**, 278–287.
51 S. R. Meyers, D. J. Kenan, X. Khoo and M. W. Grinstaff, *Biomacromolecules*, 2011, **12**, 533–539.